Published online 13 October 2016

Nucleic Acids Research, 2017, Vol. 45, No. 2 ***685–698***
doi: 10.1093/nar/gkw920

Dynamic unwrapping of nucleosomes by HsRAD51 that includes sliding and rotational motion of histone octamers

Gayan Senavirathne[1], Santosh K. Mahto[1], Jeungphill Hanne[1], Daniel O'Brian[1] and Richard Fishel[1,2,*]

[1]Department of Cancer Biology and Genetics, The Ohio State University Medical Center, Columbus, OH 43210, USA and [2]Physics Department, The Ohio State University, Columbus, OH 43210, USA

Received May 11, 2016; Revised October 01, 2016; Accepted October 10, 2016

ABSTRACT

Wrapping of genomic DNA into nucleosomes poses thermodynamic and kinetic barriers to biological processes such as replication, transcription, repair and recombination. Previous biochemical studies have demonstrated that in the presence of adenosine triphosphate (ATP) the human RAD51 (HsRAD51) recombinase can form a nucleoprotein filament (NPF) on double-stranded DNA (dsDNA) that is capable of unwrapping the nucleosomal DNA from the histone octamer (HO). Here, we have used single molecule Förster Resonance Energy Transfer (smFRET) to examine the real time nucleosome dynamics in the presence of the HsRAD51 NPF. We show that oligomerization of HsRAD51 leads to stepwise, but stochastic unwrapping of the DNA from the HO in the presence of ATP. The highly reversible dynamics observed in single-molecule trajectories suggests an antagonistic mechanism between HsRAD51 binding and rewrapping of the DNA around the HO. These stochastic dynamics were independent of the nucleosomal DNA sequence or the asymmetry created by the presence of a linker DNA. We also observed sliding and rotational oscillations of the HO with respect to the nucleosomal DNA. These studies underline the dynamic nature of even tightly associated protein–DNA complexes such as nucleosomes.

INTRODUCTION

Packaging of eukaryotic genomic DNA into histone bound nucleosomes and then into higher order chromatin structures restricts the large strings of genetic information into a very small region of space; namely the cell nucleus (1). While tight packaging reduces the chromatin volume and provides physical protection against deleterious factors, it greatly limits the accessibility of the DNA by the biological processes that maintain cells (1,2).

The repair of a dsDNA break (DSB) initially requires chromatin remodeling to remove the histones from a nearby broken end (3,4). The resulting exposed DNA may then become a substrate for the enzymatic formation of 3′ single-stranded DNA (ssDNA) tail by a 5′→3′ exonuclease and the establishment of a presynaptic ssDNA nucleoprotein filament (NPF) by RAD51 (4–6). The presynaptic RAD51 NPF performs a homology search on chromatin bound DNA that may ultimately form a transient three-stranded paranemic structure (7,8). A paired paranemic DNA within a nucleosome appears to be converted to stable plectonemic strand exchange joints by RAD54 (7,8).

The formation of the presynaptic RAD51 NPF on ssDNA appears to be the primary biologically relevant structure required for homologous recombination (HR). RAD51 NPF complexes that readily form on dsDNA *in vitro* (9–11) could be non-productive or even detrimental *in vivo* if not carefully controlled. There is evidence that BRCA2 normally prevents the progression of RAD51 filament beyond the ssDNA–dsDNA junction of processed 3′ ssDNA (12,13), and may control the nuclear localization of RAD51 following DNA damage (14). The dsDNA RAD51 NPF formed during the post-synapsis process appears to be cleared by the adenosine triphosphate (ATP)-dependent dsDNA translocation activity of RAD54 (15,16). However, misregulation of RAD51 localization (17) could lead to transient formation of a RAD51 NPF on dsDNA that might have consequences for DNA binding proteins.

Using bulk FRET analysis we showed that HsRAD51 oligomerizes onto nucleosome bound dsDNA starting from the entry-exit region and may unwrap the DNA completely from the HOs (18). These initial studies employed a HO consisting of *Xenopus laevis* histones and suggested that an HsRAD51 NPF could accomplish nucleosome remodeling *in vitro*. In addition, a simple two state kinetic model was used to describe the overall unwrapping process since pop-

*To whom correspondence should be addressed. Tel: +1 614 292 2484; Fax: +1 614 688 4994; Email: rfishel@osu.edu

ulation averaging potentially prevented the detection of any underlying intermediate states.

Here we have used single molecule imaging capable of detecting transitional states and the stochastic processes associated with HsRAD51-dependent nucleosomal DNA unwrapping. Interestingly, we observed intermediate states that appear to consist of HO rotational motion coupled to partial DNA unwrapping. These studies suggest that even a transient RAD51 NPF that forms on a nucleosome may alter histone-DNA contacts potentially enhancing a homology search and strand exchange.

MATERIALS AND METHODS

Histone expression and HO refolding

Human histones: H2A (K119C), H2B, H3 and H4 were expressed and purified from *Escherichia coli* using a slight modification of a previous protocol (19). H2A (K119C) was labeled with Cy3-maleamide (GE healthcare) in a labeling buffer containing 20 mM Tris–HCl (pH 7.0), 6 M Guanidinium hydrochloric acid and 5 mM ethylenediaminetetraacetic acid (EDTA) (20). Unreacted Cy3 was removed by sequential buffer washes with an Amicon concentrator (Millipore). Equimolar amounts of H2A (K119C), H2B, H3 and H4 were refolded into HOs and purified on a Superose12 gel filtration column (GE healthcare) as previously described (18).

Nucleosomal DNA preparation

Prior to polymerase chain reaction (PCR) amplifications of nucleosomal DNA, primers containing internal amino modified thymines (IDT, Supplementary Table S1) were labeled with Cy5-NHS ester (GE healthcare) and purified by reverse phase high-pressure liquid chromatography (RP-HPLC) on a C18 column (Agilent Technologies). Using a pair of Cy5-labled and unlabeled primers (Supplementary Table S1) with a Widom 601 nucleosome positioning sequence (601 NPS, Supplementary Table S2) containing plasmid (pDrive-601 NPS) as the template, the 601 NPS Fwd/Rev Entry-Exit–Cy5 and the 601 NPS Dyad–Cy5 DNA constructs were amplified by PCR (18). Similarly the 5S NPS Fwd Entry-Exit–Cy5 DNA construct was amplified by PCR from a plasmid (pBSII SK(-)-5S rDNA NPS) containing the *Xenopus borealis* 5S rDNA NPS sequence (Supplementary Table S2) (18). The reverse primers used in the PCRs were designed to incorporate biotin modified 78 base pair (bp) extensions to the 3′ end of each NPS (Supplementary Table S2 and Figure S1). After PCRs, the DNA constructs were purified by ion-exchange HPLC on a Gen-Pak Fax column (Waters).

Nucleosome reconstitution

Mononucleosomes were reconstituted from nucleosomal DNA and human HOs by double salt dialysis (19) followed by 5–35% sucrose gradient ultracentrifugation purification. After the purification, in order to maximize the complete localization of HO on NPS we heat shifted the samples for 2 h at 55°C (601 NPS nucleosomes) or for 30 min at 37°C (5S NPS nucleosomes) according to previously established standard heat shifting protocols (21). Purity of the nucleosome fractions was confirmed by 5% native polyacrylamide gel electrophoresis.

HsRAD51 expression and purification

In order to maximize the yield of HsRAD51 per purification, we co-expressed it with the bacterial chaperone protein GroEL. To overexpress GroEL in *E. coli*, a plasmid construct was generated as follows. First the GroEL gene was PCR amplified from pCH1-GroEL plasmid (22) using the primers described in the Supplementary Data (GroEL Forward and Reverse; Supplementary Table S1). This PCR fragment was inserted into pBAD42 backbone after digestion with the NheI and HindIII restriction enzymes. The resulting pBAD42-GroEL plasmid contained arabinose inducible GroEL with a spectinomycin resistance selection marker.

The HsRAD51 expression vector (pET 24d-HsRAD51) (10) and the GroEL expression vector (pBAD42-GroEL) harboring BLR (DE3) pLysS cells were grown at 37°C until the OD_{600} reached ∼0.3, then the GroEL expression was induced with 0.2% (w/v) L-Arabinose. After ∼30 min (when OD_{600} reach ∼0.6) HsRAD51 expression was induced by adding 0.5 mM isopropyl-β-D-thiogalactopyranoside (IPTG). Cells were harvested 4 h after the induction with IPTG, and HsRAD51 purification was carried out using the previously published sperimidine precipitation-based protocol (10,11,23) with the following modifications: in order to minimize interference from genomic DNA during the initial stage of purification we treated the cell lysates with Benzonase (50 U/ml) to completely digest the DNA. We also exchanged the order of Heparine and Cybacron Blue Agarose chromatographic steps to achieve better yields and purity of HsRAD51. Since ∼100% pure HsRAD51 was obtained without Hydroxyapatite chromatography, this step was eliminated from the purification protocol.

Single-molecule FRET experiments and data analysis

All single molecule fluorescence data in this study were acquired on a lab engineered inverted fluorescence microscope based on the Olympus IX71 body. Fluorophores were excited using the total internal reflection of the laser lines from an engineered flow cell (24). Emissions from individual complexes were achieved by the surface tethering of fluorescently tagged mononucleosomes onto a polyethylene glycol (PEG) passivated quartz surface via biotin-NeutrAvidin linkage, with a surface density of ∼0.2 molecules/μm^2. Single molecule movies with 1 Hz frame rate (with the exception of 4 Hz frame rate for the 601 NPS Rev Entry-Exit–Cy5 construct) were generated after splitting Individual Cy3 and Cy5 emissions with a Dual View optical setup (Photometrics), and recorded on an EMCCD camera (Princeton Instruments). Intensity and FRET time trajectories were processed from single molecule movies first with a custom written IDL script (24), and then with a custom written Matlab script (25,26). The apparent FRET was calculated as $I_{Cy5}/(I_{Cy3}+I_{Cy5})$. Here, I_{Cy3} is the background corrected intensity of Cy3 smoothed with a three point sliding average and I_{Cy5} is the smoothed (three point sliding average) inten-

sity of Cy5 corrected for: the background, the direct excitation by 532 nm laser and the Cy3 spectral bleed-through. All the experiments were performed at ambient temperature (21 ± 1°C). In order to compensate for the reduced activity of HsRAD51 at this lower temperature we used ∼2–3-fold higher protein concentrations compared to our previous studies (18), which were performed at 37°C temperature.

Single-molecule photobleaching analysis

We first characterized the wrapping state of individual mononucleosomes tethered on the surface by carrying out photobleaching of Cy3 and Cy5. This was done by illumination of ∼4 mm^2 of the sample chamber with a green laser (532 nm, ∼2.5 mW) at ∼0.6 mW/mm^2. The imaging buffer contained 30 mM Tris–HCl pH 7.5, 110 mM KCl, 10 mM NaCl, 2 mM $MgCl_2$, 0.1 mM dithiothreitol (DTT), 30 μM EDTA, 0.2 mg/ml bovine serum albumin, 0.02% (w/v) IGPEPAL, 1% (w/v) sucrose (Buffer I) supplemented with a photo-stability and oxygen scavenging (POS) cocktail containing saturated (∼3 mM) Trolox to prevent the photoblinking of the fluorophores, with the protocatechuic acid (PCA)-protocatechuate-3,4-dioxygenase (PCD) oxygen scavenger system composed of PCA (5 mM) and PCD (0.05 U/ml; rPCO; OYC Americas) (27) to slow the rate of photobleaching. For each experiment, four to five ∼10 min long single molecule movies were recorded from multiple areas of the engineered flow cell channels. Since we observed unusually rapid photobleaching for the 601 NPS Rev Entry-Exit–Cy5 Nuc construct under these regular photobleaching solution conditions, PCD concentration was increased to 0.21 U/ml and four to five ∼5 min long single molecule movies were recorded at 250 ms (4 hz) time resolution. During the data analysis photobleaching molecules were readily identified by abrupt irreversible disappearance of the fluorescence and categorized based on the number of observed Cy3 bleaching steps as well as apparent FRET values.

HsRAD51 catalyzed nucleosome remodeling experiments

To examine HsRAD51 catalyzed nucleosome remodeling, mononucleosomes were immobilized on the surface in Buffer I supplemented with POS (∼3 mM Trolox, 5 mM PCA and 0.21 U/ml PCD (27)) and 0.5 mM ATP as described above. Data acquisition was initiated by exciting ∼4 mm^2 area of the sample chamber with a green laser (532 nm, ∼1.5 mW) at ∼0.4 mW/mm^2. Recording was started without HsRAD51 and after ∼60 s HsRAD51 in Buffer I plus POS with 0.5 mM ATP was infused into the flow cell chamber. The recording was continued for ∼18 min and the excitation was switched to a red laser (635 nm; 0.5 mW/mm^2) for ∼30 s before ending the recording. Control experiments were carried out similarly, albeit with HsRAD51 only or ATP only. We determined the necessity of HsRAD51 catalyzed ATP hydrolysis for nucleosome remodeling by replacing Mg^{2+} with the same concentration of Ca^{2+} and replacing ATP with the same concentration of adenosine diphosphate (ADP) or ATPγS in the Buffer I as indicated.

Since we observed rapid photobleaching for the 601 NPS Rev Entry-Exit–Cy5 construct under the regular remodeling solution conditions PCD concentration was increased to 0.42 U/ml. Single molecule imaging was done only for 10 min total time span where the real time infusions were done at ∼30 s and the direct red laser excitation was done during the last 10 s. For all the remodeling experiments data for individual molecules were obtained from the single molecule movies (one movie per reaction chamber) as described above and processed exactly in the same way, with the exception that we selected only high FRET trajectories for further analyses.

Single-molecule salt jump experiments

Similar to the HsRAD51 remodeling experiments, salt jump experiments were performed by the real time infusion of the Buffer I (without KCl) supplemented with 800 or 1600 mM NaCl on to the surface immobilized mononucleosomes that were initially maintained in Buffer I supplemented with POS. In order to insure that the observed intensity and FRET decay were due to histone disassembly, but not due to fluorophore photobleaching, the high salt concentrations in Buffer I were adjusted by using small volumes 5 M NaCl after depleting the oxygen with the POS without the salt. The real time injections were done 60 s after commencing the measurements, and the recordings were continued until 10 min whereupon the laser excitation was switch from green to red for another 2 min. The survival of Cy5 fluorescence (∼100% of the molecule) during the entire direct excitation period indicates that the zero FRET is not originating from Cy5 photobleaching and our observations are not obscured or limited by the fluorophore photobleaching.

Population analysis of FRET trajectories

A small percentage (<5%) of trajectories obtained with HsRAD51 alone or ATP alone showed short lived, isolated, abrupt FRET transitions directly to zero FRET as a result of occasional Cy5 photoblinking. These events were not considered as HsRAD51 induced nucleosome-remodeling events, which usually consisted of intermediate steps. To categorize individual time trajectories as static or dynamic, a population analysis was done by manually counting individual molecules. A FRET trajectory that showed at least one clear anti-correlated transition which deviate more than two standard deviations (>2 σ) from the initial FRET was counted as a dynamic molecule (28). We used the standard deviation (σ, usually ∼0.05 ± 0.01) of the FRET histograms built from the control experiments as the reference for this analysis. Static trajectories did not show such FRET fluctuations that resulted from anti-correlated changes of Cy3 and Cy5 intensities, except for occasional photoblinking as described above. The total number of molecules analyzed for each experiment is denoted as N, while the number of dynamic molecules is denoted as n.

Post-synchronization and histogram analysis of FRET trajectories

Individual trajectories were truncated prior to the photobleaching of Cy3, to construct post-synchronized FRET

densities consist of 0.05 FRET bins and 1 s time bins (250 ms time bins for 601 NPS Rev Entry-Exit–Cy5 Nuc construct). The 0.05 FRET threshold was used to align all trajectories with respect to the beginning of the movies using a custom written MatLab code (25,26). Time averaged FRET histograms were generated by compiling individual trajectories in IGOR Pro (Wavemetrics, Lake Oswego, OR, USA) (25,26), and fitted with single or sum of multiple Gaussians as indicated in the figures.

Hidden markov model (HMM) analysis of the dynamic FRET trajectories

Dynamic FRET trajectories were subjected to idealization by a maximum likelihood-based Hidden markov model (HMM) analysis using the HaMMy software (25,29). These idealized FRET trajectories were compiled to build transition density plots (TDP), which show the number of transitions between a given initial FRET state and a final FRET state as a two-dimensional heat map. Since we observed numerous FRET levels in time trajectories, and in order not to constrain the analysis to predetermined number of canonical states, we used the maximum number of available 10 states as the initial guess. The software is designed to chose the optimum number of states without over fitting the data as a result of the built-in Bayesian criterion (29). Manual inspection of different initial guesses, e.g. 2, 4, 6, 8 and 10 states confirmed the accuracy of using 10 as the initial guess.

RESULTS

Visualization and characterization of individual nucleosomes by smFRET

To visualize individual surface tethered mononucleosomes consisting of human histones and the 601 NPS or 5S rDNA NPS (5S NPS), we tagged the H2A histone with Cy3, and the DNA with Cy5 at the entry-exit regions (Fwd/Rev Entry-Exit–Cy5 Nucs; Figure 1A, C and E; Supplementary Figure S1A and B) or at the dyad region (Dyad–Cy5 Nuc; Figure 1G and Supplementary Figure S1C). Cy5 was placed on the DNA, such that the FRET between Cy3 and Cy5 would report the wrapping state of the nucleosome (18,30,31). In a single molecule photobleaching experiment ('Materials and Methods' section) (30,31), 601 NPS Fwd Entry-Exit–Cy5 Nuc showed three types of FRET trajectories with three different static FRET levels (Figure 1B and Supplementary Figure S2A1–D1). The high-FRET state ($E_{P\bullet 601FEE} = 0.95$) was more prominent, and intensity trajectories that constituted this subpopulation showed a single Cy3 photobleaching event (Supplementary Figure S2A1). These observations indicate the presence of a single Cy3-H2A located proximal (P) to the Cy5 on the DNA. Similarly the low-FRET state ($E_{D\bullet 601FEE} = 0.25$) resulted from one Cy3 molecule located distal (D) to the Cy5 on the DNA (Supplementary Figure S2B1). A mid-FRET state ($E_{M\bullet 601FEE} = 0.60$) was an indicator of a mixed (M) FRET state, with the trajectories containing two Cy3 photobleaching events. These two events could easily be characterized as photobleaching of a D-Cy3 that resulted in the formation of a P-Cy3 FRET state or vice versa (Supplementary Figure S2C1 and D1). Thus, the M-FRET state represents mononucleosomes containing two Cy3-labeled H2A monomers within the HO. Replacing the 601 NPS in the Fwd Entry-Exit–Cy5 Nuc with the 5S NPS resulted in slightly broader, otherwise nearly identical photobleaching FRET distributions that consist of three FRET states ($E_{P\bullet 5SFEE} = 0.95$, $E_{D\bullet 5SFEE} = 0.27$, $E_{M\bullet 5SFEE} = 0.68$) (Figure 1D and Supplementary Figure S2A2–D2).

Similarly, a 601 NPS Rev Entry-Exit–Cy5 Nuc construct generated by moving the Cy5 fluorophore in 601 NPS Fwd Entry-Exit–Cy5 Nuc in to the opposite entry-exit region resulted in three broad photobleaching FRET peaks ($E_{P\bullet 601REE} = 0.80$, $E_{D\bullet 601REE} = 0.19$, $E_{M\bullet 601REE} = 0.39$) (Figure 1F and Supplementary Figure S2A3–D3). However, careful analysis of individual photobleaching events revealed that ∼25% of the mononucleosomes containing a single Cy3 showed partial positioning of HO on NPS. These resulted in an intermediate (∼0.50) FRET value that did not resolve in to P or D states but rather contributed to the M state of the overall FRET distribution. Furthermore, we identified these partially positioned nucleosomes as the main source of broadening of the FRET distributions in contrast to the previous two constructs.

Photobleaching studies performed on the 601 NPS Dyad–Cy5 Nuc showed very similar characteristics, albeit with slightly different FRET states that resulted from different inter-fluorophore distances (Figure 1H and Supplementary Figure S2A4–D4). The assignment of FRET values: ($E_{P\bullet 601D} = 0.72$, $E_{D\bullet 601D} = 0.26$, $E_{M\bullet 601D} = 0.47$) follows the same reasoning presented above. Together, these data show that all four mononucleosome FRET constructs used here can give rise to multiple different FRET states, and unlike in ensemble level experiments (18) we can unambiguously select individual molecules for further analysis to accurately study the nucleosome remodeling processes.

HsRAD51 alters nucleosome dynamics when reported from the entry-exit region

To visualize nucleosome dynamics in real time, we introduced HsRAD51 with ATP onto the surface immobilized 601 NPS Fwd Entry-Exit–Cy5 Nuc (Figure 2A). In this arrangement we expect that the formation of an HsRAD51-dsDNA NPF starting from the entry-exit region will ultimately result in displacement of the 601 NPS DNA from the HO surface while simultaneously lengthening the DNA by ∼50% (9,18). As a consequence the Cy3-Cy5 inter-fluorophore distance should increase resulting in a corresponding decrease in observed FRET (18). From the three possible FRET trajectories (P, D, M; Figure 1B and Supplementary Figure S2), we selected only initial high FRET states ($E_{P\bullet 601FEE} \geq 0.95$) for further analysis since these molecules *a priori* contain clearly localized HO with respect to the 601 NPS, allowing unambiguous assignment of catalytic intermediates. The real-time infusion of ATP or HsRAD51 alone into the flow cell resulted in static FRET trajectories for all of the tracked molecules ($N = 93$ for ATP, $N = 82$ for HsRAD51) that lasted the entire observation period (∼20 min; Figure 2B; Supplementary Figure S3A and B, left panels). Moreover, these trajectories resulted in narrower static FRET densities (Supplementary Figure S3A and B, right panels) suggesting that the mononucleosomes

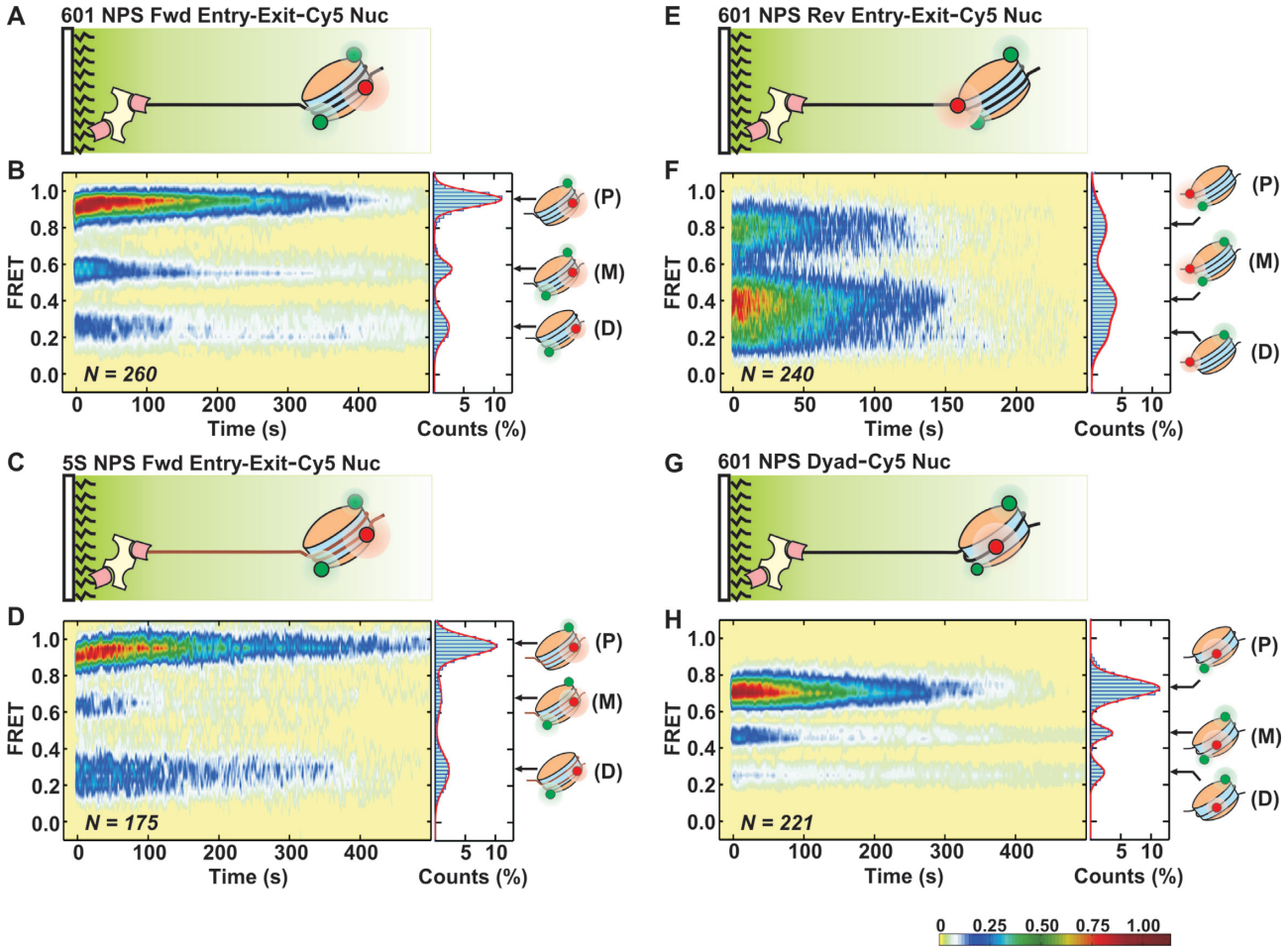

Figure 1. Nucleosome constructs consist of three FRET species. (**A**) An illustration of the single molecule photobleaching experimental setup for 601 NPS Fwd Entry-Exit–Cy5 Nuc construct. HO (H2A-H2B orange, $(H3\text{-}H4)_2$ light blue) is labeled with Cy3 (green circles) at H2A and either both or one of the H2A may contain Cy3. The DNA (black line) is immobilized on PEG (black wavy lines) passivated quartz surface via biotin (pink rectangle)-NeutrAvidin (yellow rectangle) interactions. (**B**) The post-synchronized FRET density plot and the corresponding time-averaged FRET histogram for photobleaching of $N = 260$ molecules, showing three discrete FRET states identified as Proximal (P), Distal (D) and Mixed (M). A Gaussian fit to the time averaged FRET, which consists of the sum of three Gaussian functions is shown as a red line. (**C**) An illustration of the single molecule photobleaching experimental setup for 5S NPS Fwd Entry-Exit–Cy5 Nuc construct. (**D**) The Post-synchronized FRET density plot and the corresponding FRET histogram for photobleaching of $N = 175$ molecules showing three discrete FRET states identified as Proximal (P), Distal (D) and Mixed (M). A Gaussian fit to the time averaged FRET, which consists of the sum of three Gaussian functions is shown as a red line. (**E**) An illustration of the single molecule photobleaching experimental setup for 601 NPS Rev Entry-Exit–Cy5 Nuc construct. (**F**) The Post-synchronized FRET density plot and the corresponding FRET histogram for photobleaching of $N = 240$ molecules showing three discrete FRET states identified as Proximal (P), Distal (D) and Mixed (M). A Gaussian fit to the time averaged FRET, which consists of the sum of three Gaussian functions is shown as a red line. (**G**) An illustration of the single molecule photobleaching experimental setup for 601 NPS Dyad–Cy5 Nuc construct. (**H**) The Post-synchronized FRET density plot and the corresponding FRET histogram for photobleaching of $N = 221$ molecules showing three discrete FRET states identified as Proximal (P), Distal (D) and Mixed (M). A Gaussian fit to the time averaged FRET, which consists of the sum of three Gaussian functions is shown as a red line. The intensity bar indicates the relative frequencies of FRET values in post-synchronized FRET density plots (low = yellow, high = red).

were exceptionally stable on the PEG passivated surface under these largely physiological ionic conditions.

Introduction of HsRAD51 (250 nM) with ATP (0.5 mM) resulted in 46% of dynamic trajectories displaying at least one clear anti-correlated FRET transition to a lower FRET state ($E_{RAD51} < 0.95$; 'Materials and Methods' section, Figure 2B and C, Supplementary Figure S4A). The dwell times for the anti-correlated lower FRET states ranged from ∼1 s to a few minutes. These observations are consistent with the conclusion that nearly half of the nucleosomes were undergoing a dynamic remodeling process.

We also observed synchronized dynamic trajectories that resulted in a much broader FRET density, which encompassed the entire dynamic range of FRET (compare Figure 2C and Supplementary Figure S3) (25,26). Although dynamic nucleosome behavior was apparent within a few seconds following the HsRAD51 and ATP infusion, FRET excursions became more pronounced after ∼400 s (Figure 2C, right panel). Increasing the concentration of HsRAD51 to 500 nM resulted in an associated increase in the fraction of dynamic FRET trajectories to a saturated level of 96% (Figure 2B). These trajectories represented both an increase in the amount of FRET transitions per dynamic tra-

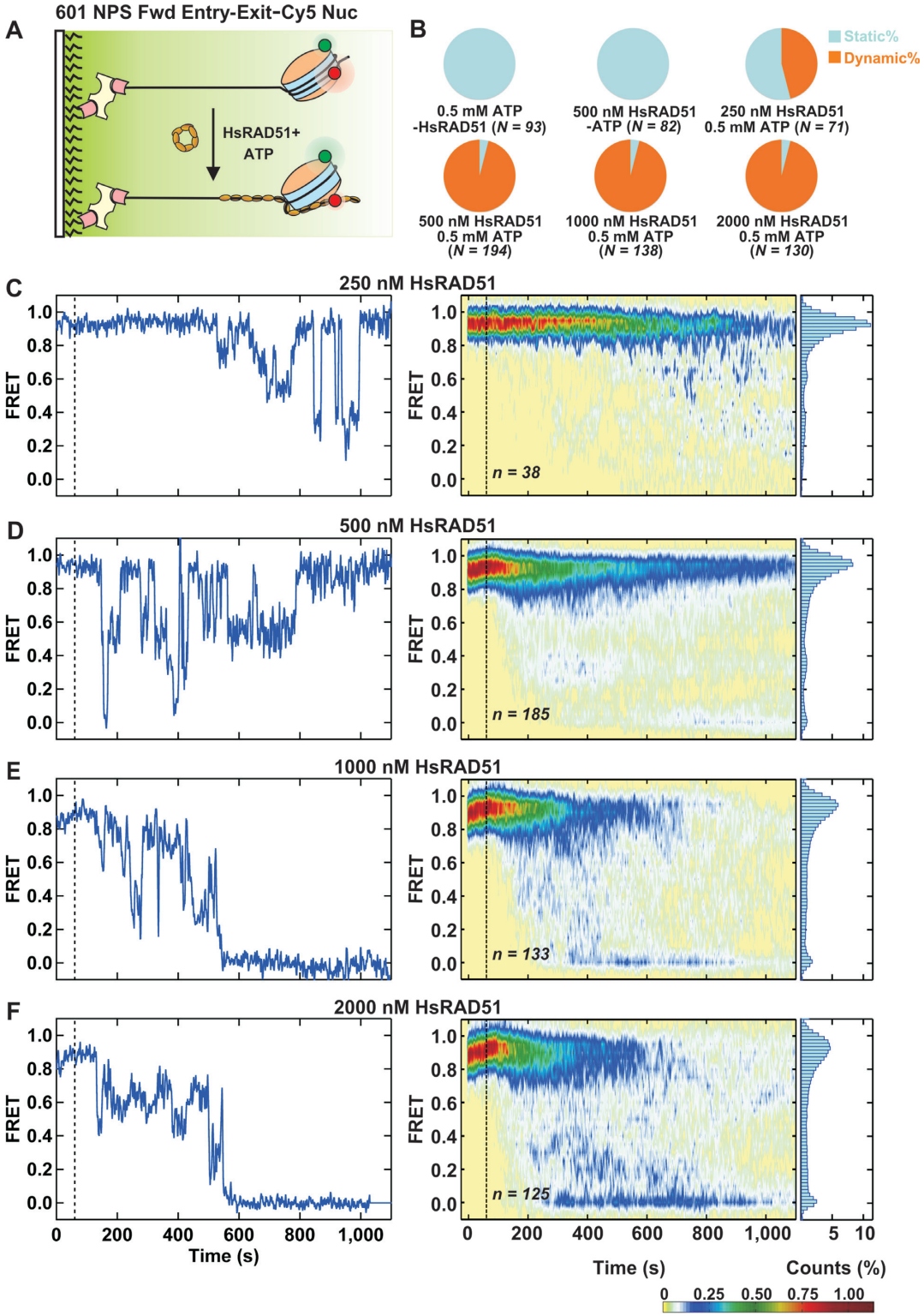

Figure 2. Visualizing the nucleosomal DNA unwrapping by HsRAD51 from the entry-exit region. (**A**) An illustration of the single molecule mononucleosome experimental setup to visualize HsRAD51 catalyzed nucleosome remodeling relative to the entry-exit region. Increasing concentrations (250–2000 nM) of HsRAD51 with 0.5 mM ATP were introduced onto surface immobilized mononucleosomes. (**B**) Population analysis showing the percentages of static and dynamic molecules obtained at the indicated experimental conditions. The total number of molecules (*N*) analyzed for each experiment is also shown at the bottom of the corresponding pie chart. (**C**–**F**) Representative single molecule dynamic FRET trajectories, post-synchronized FRET density plots and time averaged FRET histograms for all the HsRAD51 concentrations tested. HsRAD51 concentration and the number of molecules (*n*) analyzed are indicated in each panel. Real time infusion of HsRAD51 and ATP is marked by vertical dotted lines at 60 s. The intensity bar indicates the relative frequencies of FRET values in post-synchronized FRET density plots (low = yellow, high = red). Cy3, Cy5 Intensity trajectories corresponding to above FRET trajectories are shown in Supplementary Figure S4.

jectory and the rate of onset of FRET dynamics (Figure 2D and Supplementary Figure S4B). Interestingly, the residence times in low FRET states ($E_{RAD51} < 0.95$) did not change appreciably compared to lower HsRAD51 concentration (250 nM; Figure 2C and D). Further increasing the concentration of HsRAD51 to 1000 and 2000 nM resulted in similar fluorescence and FRET time trajectories, albeit with generation of frequent zero or near zero FRET states that are indicative of recurrent DNA movement of ≥100 Å away from the HO surface (Figure 2E and F; Supplementary Figure S4C and D) (30). Direct excitation of Cy5 with a red (635 nm) laser at the end of each observation allowed us to confirm that zero FRET was not a result of Cy5 photobleaching (Supplementary Figure S4C and D). Interestingly, a subset of trajectories showed loss of Cy3 fluorescence following the formation of a zero or near zero FRET state (Supplementary Figure S5). We interpret most of these to represent the loss of Cy3-labeled H2A-H2B dimer or the entire HO from the DNA (18,32). However, we cannot formally rule out the possible loss of Cy3 signal as a result of photobleaching.

Careful inspection of individual single molecule trajectories and resulting FRET density plots showed that partially unwrapped states did not fall into quantized FRET levels, rather they represented a continuum of FRET values ranging from FRET zero to 1 (Figure 2C–F). Consistent with this observation, a TDP compiled by HMM analysis of FRET trajectories (25,29) did not show discrete peaks and displayed two continuous diagonal 'lobes' (Supplementary Figure S6). Together these data suggest a mechanism in which stochastic oligomerization of HsRAD51 onto the DNA (9) leads to stepwise but stochastic removal of the DNA from the HO.

Deconvolution of the HsRAD51 catalyzed DNA unwrapping and histone disassembly

To gain further insights in to the mechanism of histone disassembly during HsRAD51 NPF formation, we subjected surface tethered 601 NPS Fwd Entry-Exit–Cy5 Nuc to real time single molecule salt jump experiments using two 'high' salt concentrations. These salt concentrations are known to evict primarily $(H2A\text{-}H2B)_2$ (800 mM NaCl) or the entire HO (1600 mM NaCl) from 601 NPS ('Materials and Methods' section) (32). Interestingly, immediately following the introduction of 800 mM NaCl we observed salt induced FRET transitions where loss of Cy3 signal occurred via a transient ∼0.3 FRET (90% of the molecules) or a zero FRET (10% of the molecules) state, indicating the transient unwrapping of DNA away from H2A prior to the eviction of $(H2A\text{-}H2B)_2$ from the DNA (Supplementary Figure S7A–C) (32). Increasing the exchanged NaCl concentration to 1600 mM increased the rate of FRET decay where 100% of the molecules loss Cy3 signal through a highly short-lived zero FRET state indicating fast removal NPS DNA from HO (Supplementary Figure S7D–F) (32) momentarily followed by the complete dissociation of HO. The presence of long lasting active Cy5 during the direct excitation with the red (635 nm) laser indicated that zero FRET was not caused by Cy5 photobleaching and fluorescent dyes are photo-stable at high ionic conditions.

Although mononucleosomal disassembly dynamics observed in the presence of high salt is fundamentally different from HsRAD51 catalyzed nucleosome remodeling kinetics (compare Figure 2C–F and Supplementary Figure S7), we note that the final stage of HsRAD51 catalyzed nucleosome remodeling is analogous to that of the salt induce H2A-H2B and/or HO eviction (compare Supplementary Figures S5 and S7) further supporting a mechanism by which the gradual formation of HsRAD51 NPS leading to the complete removal of histones from NPS DNA.

Function of ATP hydrolysis by HsRAD51 during nucleosome remodeling

Although we have previously shown that ATP hydrolysis by HsRAD51 is essential for its nucleosome remodeling activity (18), the ensemble averaged asynchronous kinetics did not permit us to locate the exact ATP hydrolysis step. Because in the current study we are able to visualize the individual nucleosomes as they undergo remodeling in real time, we can locate the ATP hydrolysis step with a high certainty. For these studies we replaced the 'regular' ATP ($ATP.Mg^{2+}$) with $ADP.Mg^{2+}$, $ATP.Ca^{2+}$ or $ATP\gamma S.Mg^{2+}$ as nucleotide cofactors in the presence of 500 nM HsRAD51 and carried out real time remodeling experiments using the 601 NPS Fwd Entry-Exit–Cy5 Nuc construct ('Materials and Methods' section).

Despite the ability of HsRAD51 to oligomerize on ds-DNA in the presence of $ADP.Mg^{2+}$ or $ATP.Ca^{2+}$ (9) we did not observe any nucleosome remodeling activity in the presence these two nucleotide cofactors (Supplementary Figure S8A–C). However, we only observed efficient nucleosome remodeling activity in the presence of ATP ($ATP.Mg^{2+}$) (compare Figure 2B and D with Supplementary Figure S8A–C). Moreover, the experimental construct used here should report any distance change occurs in the entry-exit region and therefore even the early steps of the nucleosome remodeling process. Thus, these observations strongly suggest that ATP hydrolysis is required from the initiation of the reaction.

When we replaced the $ATP.Mg^{2+}$ with weakly hydrolysable $ATP\gamma S.Mg^{2+}$ (11) we observed a substantial reduction in the number of mononucleosomes that underwent dynamic remodeling processes (95% for $ATP.Mg^{2+}$ and 56% for $ATP\gamma S.Mg^{2+}$, compare Figure 2B with Supplementary Figure S8A) as well as the rate of FRET decay onset (∼50 s for $ATP.Mg^{2+}$ and ∼400 s for $ATP\gamma S.Mg^{2+}$, compare Figure 2D with Supplementary Figure S8D). In summary these data are constant with a hypothesis that ATP hydrolysis by HsRAD51 is required to initiate the nucleosome remodeling process.

HsRAD51 induced stochastic nucleosome dynamics are independent of the NPS sequence

Because the 601 NPS was artificially selected for a strong HO positioning ability (33,34) it is formally possible that the DNA sequence itself might contribute to the stochastic fluctuations observed in our single molecule analysis. To rule out this and to further extend our analysis to biologically relevant DNA sequences we replaced the 601 NPS

from Fwd Entry-Exit–Cy5 Nuc by a 147 bp DNA sequence present within *X. borealis* 5S rDNA NPS that has weaker interaction with HO (5S NPS Fwd Entry-Exit–Cy5 Nuc, Figure 1C, Supplementary Table S2, Supplementary Figure S1A, 'Materials and Methods' section) (18).

Out of three possible FRET trajectories (P, D, M; Figure 1D and Supplementary Figure S2) we selected only high initial FRET (P) subpopulation ($E_{P\bullet 5SFEE} > 0.95$) to characterize the nucleosome remodeling dynamics. The residual amounts (<5%) of slow nucleosome dynamics observed in the presence of either HsRAD51 or ATP alone (Figure 3A; Supplementary Figure S9A and B) is consistent with the weaker affinity of 5S NPS for HO. However, the introduction of HsRAD51 with ATP induced faster dynamics in 100% of the mononucleosomes (Figure 3A and B). We also note that the basic characteristics of the remodeling process such as reversibility and stochastics are well conserved in this nucleosome construct compared to the 601 NPS Fwd Entry-Exit–Cy5 Nuc construct, in spite of somewhat faster completion of the reaction (compare Figure 2B and D with Figure 3A and B). Together these data confirm our hypothesis that the stochastic oligomerization of HsRAD51 leads to stepwise but stochastic removal of the nucleosomal DNA from the HO regardless of the NPS DNA sequence.

HsRAD51 can oligomerize on nucleosomal DNA from both entry-exit sides and catalyze nucleosome remodeling equally well

The sequence asymmetry present in 601 NPS combined with the inherent asymmetry posed by the extra 78 bp DNA linker present in our smFRET experimental setup raise an important question whether the observations made on Fwd Entry-Exit–Cy5 mononucleosomes are applicable to the remodeling from the opposite entry-exit direction. We sought to answer this question by moving the Cy5 fluorophore in the forward entry-exit side to the reverse entry-exit side where the extra 78 bp linker DNA is located (601 NPS Rev Entry-Exit–Cy5 Nuc, Figure 1E, Supplementary Figure S1B, 'Materials and Methods' section).

Much to our surprise we observed that the Cy5 fluorophore in this location is greatly compromising the correct localization of HO by NPS (Figure 1F). Furthermore, possible alterations in the microenvironment appeared to result in much faster photobleaching of Cy3 fluorophores on H2A even under the photo-protective conditions ('Materials and Methods' section). These effects inhibited our ability to visualize the complete remodeling process with this nucleosome construct. However, imaging at high temporal resolution (250 ms) allowed us to examine at least the initial stage of remodeling in details ('Materials and Methods' section). Control experiments performed with HsRAD51 alone or ATP alone revealed nearly static mononucleosomes (Supplementary Figure S9C). These nucleosomes became highly dynamic by the presence of 500 nM HsRAD51 and ATP (Figure 3C). Interestingly, the single molecule trajectories and the FRET densities showed clear resemblance to those of the 601 NPS Fwd Entry-Exit–Cy5 Nuc mononucleosomes (compare Figures 2D and 3C). These results indicate that regardless of the linker DNA, HsRAD51 can oligomerize on to the reverse entry-exit region of the nucleosomal DNA and hence catalyze the nucleosomes remodeling. This observation is in clear agreement to our previous ensemble level studies that showed the linker DNA has no apparent effect on the nucleosome remodeling activity of HsRAD51 (18). Compared to the forward construct, seemingly faster accumulation of zero FRET state with active Cy5 fluorophores (100% of $n = 10$ molecules), indicated a faster unwrapping of DNA from the reverse entry-exit side. This is consistent with the lower stability of the right half of the 601 NPS compared to the left half (34,35).

Taken together our data show that HsRAD51 can oligomerize on nucleosomal DNA from both the entry-exit sides and therefore can catalyze remodeling equally well regardless of the presence of a linker DNA or other structural and sequence asymmetries.

HsRAD51 alters nucleosome dynamics when reported from the dyad region

Our previous studies indicated a clear kinetic difference in nucleosome unwrapping when the entry-exit and dyad regions of the nucleosome were compared (18). To determine whether a similar stochastic processes occur throughout the nucleosome during HsRAD51-dependent unwrapping, we examined FRET transition between the Cy3-labeled H2A within the HO and a Cy5 label located in the dyad region of the NPS (601 NPS Dyad–Cy5 Nuc, Figure 4A) (18). FRET trajectories were selected with initial high FRET ($E_{P\bullet 601D} \geq 0.72$) where the Cy3-H2A is located proximal (P) to the Cy5 on the NPS DNA. As controls we found that HsRAD51 or ATP alone displayed static FRET trajectories that spanned the entire observation period of ∼20 min (Figure 4B and Supplementary Figure S10). These observations indicate there was no remodeling and that the nucleosomes are stable during the entire incubation period.

The introduction of HsRAD51 in the presence of ATP induced dynamic FRET trajectories in the 601 NPS Dyad–Cy5 Nuc that were dependent upon protein concentration (Figure 4B–F). As might be expected, the fraction of dynamic FRET trajectories at any specific HsRAD51 concentration was less than that for the 601 NPS Fwd Entry-Exit–Cy5 Nuc at the same protein concentration (compare Figures 2B and 4B). Thus, the smFRET data appear generally consistent with our previous bulk analysis of nucleosome unwrapping (18). However, we noted numerous FRET transitions that consisted of frequent upturns relative to the initial high FRET state (Figure 4C–F, $E_{RAD51} > 0.72$). Moreover, at lower HsRAD51 concentrations (250, 500 nM) the FRET appeared to oscillating rapidly (∼1 s^{-1}) between elevated and low levels, while the average remained centered around the initial high FRET (E ∼0.72; Figure 4C and D; Supplementary Figure S11A and B). These FRET transitions clearly contrasted the expected FRET decreases associated with a pure NPS DNA unwrapping mechanism, where only an increase in inter-fluorophore distance was expected due to the removal of the DNA from the HO surface and lengthening of the DNA by ∼50% (18). Careful inspection of the HO footprint on the 601 NPS along with the relative locations of the fluorophores (Supplementary Figure S1C, bottom panel) seems to indicate that the FRET increases relative to the initial 0.72 value is due to

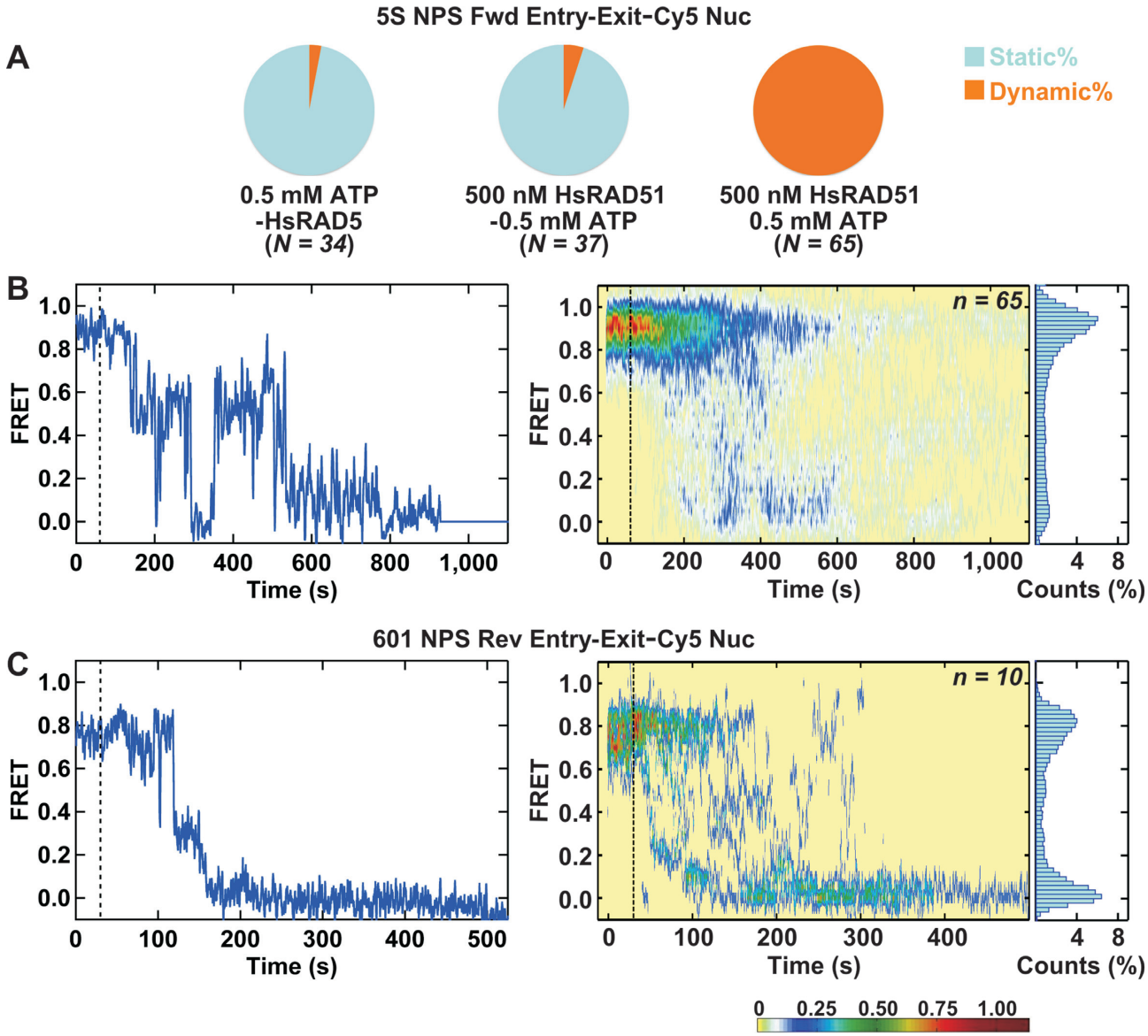

Figure 3. The mechanism of nucleosomal DNA unwrapping by HsRAD51 does not depend on the sequence and the asymmetry of NPS DNA. (**A**) Population analysis showing the percentages of static and dynamic molecules obtained at the indicated experimental conditions for 5S NPS Fwd Entry-Exit–Cy5 Nuc construct. The total number of molecules (*N*) analyzed for each experiment is also shown at the bottom of the corresponding pie charts. (**B**) A representative single molecule dynamic FRET trajectory, the post-synchronized FRET density plot and the time averaged FRET histogram obtained at 500 nM HsRAD51 for 5S NPS Fwd Entry-Exit–Cy5 Nuc construct. (**C**) A representative single molecule dynamic FRET trajectory, the post-synchronized FRET density plot and the time averaged FRET histogram obtained at 500 nM HsRAD51 with high (250 ms) temporal resolution for 601 NPS Rev Entry-Exit–Cy5 Nuc construct. The smFRET experimental constructs used in these studies are analogous to Figure 2A, and the numbers of molecules (*n*) analyzed are indicated in each panel. The vertical dotted lines at 60 s in (B) and 30 s in (C) indicate the real time infusion of HsRAD51 with ATP. The intensity bar indicates the relative frequencies of FRET values in post-synchronized FRET density plots (low = yellow, high = red).

the movement of P-Cy3-H2A closer to the Cy5 on the NPS DNA by the sliding/rotation of the HO. This observation seems to additionally suggest that rapid FRET oscillation observed above should be originating from short range HO sliding/rotational oscillations with respect to the dyad DNA.

When the concentrations of HsRAD51 was increased to 1000 and 2000 nM with the 601 NPS Dyad–Cy5 Nuc, the fast FRET oscillations appeared to convert into slower but larger FRET transitions similar to that of the 601 NPS Fwd Entry-Exit–Cy5 construct (Figure 4E and F; Supplementary Figure S11C and D). These results suggest that large-scale DNA movements become dominant over the small-scale HO movements. Interestingly, these larger FRET transitions still contain numerous small FRET oscillations within them (Figure 4E and F; Supplementary Figure S11C and D), suggesting that residual HO movements may be coupled to the DNA unwrapping-rewrapping as shown in a recent theoretical study (36).

For both the 601 NPS Fwd Entry-Exit–Cy5 Nuc and 601 NPS Dyad–Cy5 Nuc constructs, larger FRET dynamics were reversible until the generation of zero FRET state.

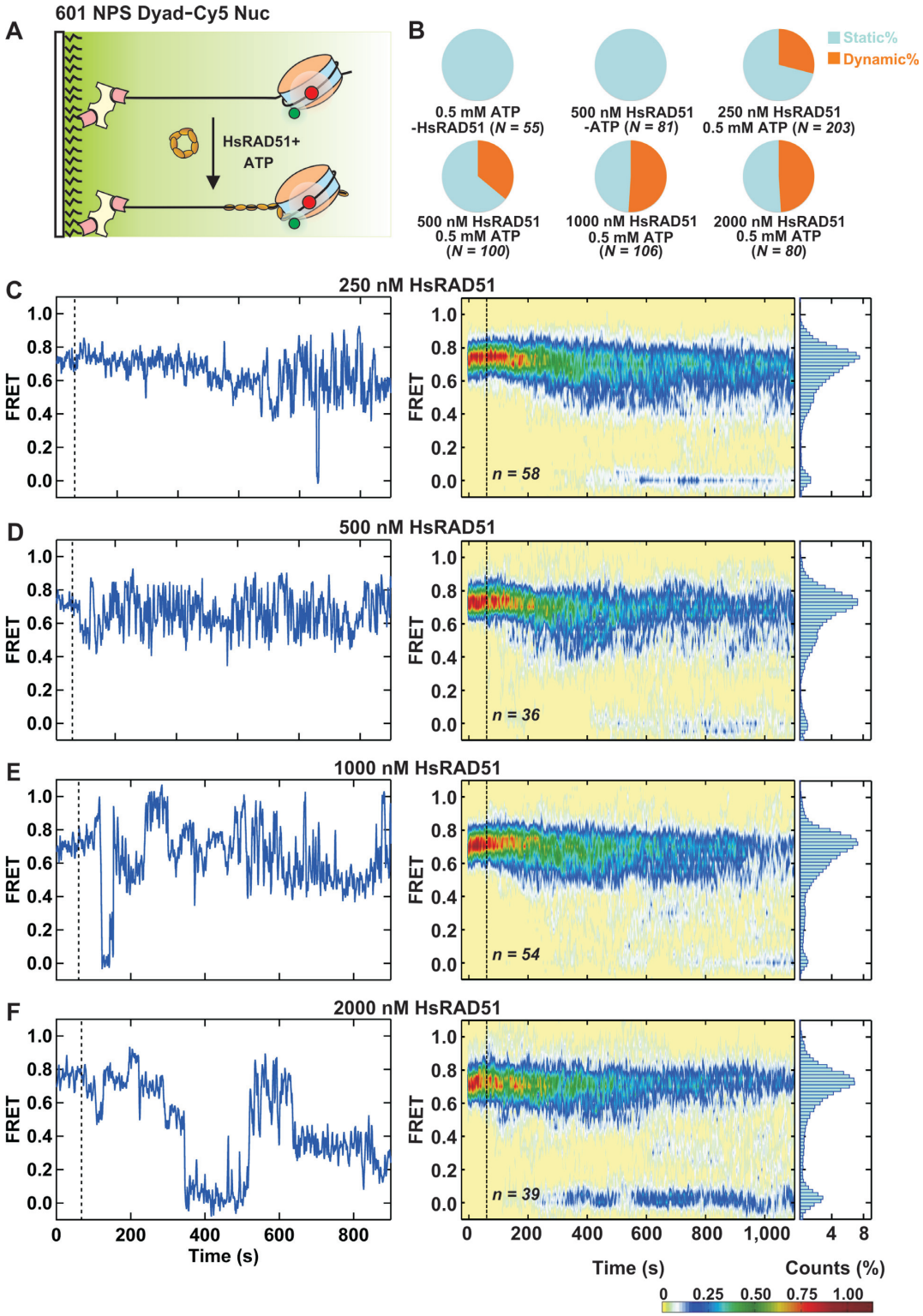

Figure 4. Visualizing HO sliding/rotation-coupled nucleosomal DNA unwrapping by HsRAD51. (**A**) An illustration of the single molecule mononucleosome experimental setup to visualize HsRAD51 catalyzed nucleosome remodeling relative to the dyad region. Increasing concentrations (250–2000 nM) of HsRAD51 with 0.5 mM ATP were introduced onto surface immobilized mononucleosomes. (**B**) Population analysis showing the percentages of static and dynamic molecules obtained at indicated experimental conditions. The total number of molecules (*N*) analyzed for each experiment is also shown at the bottom of the corresponding pie chart. (**C**–**F**) Representative single molecule dynamic FRET trajectories, post-synchronized FRET density plots and time averaged FRET histograms for all the HsRAD51 concentrations tested. HsRAD51 concentration and the number of molecules (*n*) analyzed are indicated in each panel. Real time infusion of HsRAD51 and ATP is marked by vertical dotted lines at 60 s. The intensity bar indicates the relative frequencies of FRET values in post-synchronized FRET density plots (low = yellow, high = red). Cy3, Cy5 Intensity trajectories corresponding to above FRET trajectories are shown in Supplementary Figure S11.

During this time we observe the occasional loss of Cy3 (Figures 2 and 4; Supplementary Figures S4, 5, 11 and 12), which we interpret as the dissociation of $(H2A\text{-}H2B)_2$ or complete eviction of the entire HO. These results are consistent with the conclusion that HsRAD51 NPF formation within the nucleosome results in dynamic unwrapping and rewrapping 'tug-of-war' with the NPS DNA that eventually results in the complete and irreversible loss of Cy3-H2A or HO (Figure 5) (18,32).

Deconvolution of HsRAD51 catalyzed DNA unwrapping and HO sliding/rotational motion

To further characterize the HO sliding/rotation mechanism, we overlaid the smFRET histograms obtained from the remodeling experiments with histograms obtained from the control experiments for 601 NPS Dyad–Cy5 Nuc P-Cy3 subpopulation (Supplementary Figure S13A–D). The broadening of the histograms in the remodeling experiments compared to that of controls clearly indicates the dynamic remodeling of nucleosomes. The broadening toward the low FRET (left) side mainly originates from DNA unwrapping and the broadening toward high FRET (right) side indicates the motion of HO with respect to the dyad (see the fluorophore locations in Supplementary Figure S1C, bottom panel). The asymmetry created by the initial high FRET combined with the tendency of the reaction to move toward the low FRET regime, due to DNA unwrapping and lengthening, appears to under estimate the right side broadening of the remodeling FRET histograms. However we still observed a significant fraction of broadening toward the high FRET side that appears to increase with increased HsRAD51 concentrations (Supplementary Figures S13A–D). This observation is consistent with the frequent and long dwelling high FRET ($E_{RAD51} > 0.72$) transitions observed at elevated protein concentrations (Figure 4E and F; Supplementary Figure S11C and D).

In order to relieve the asymmetric bias created by the initial high FRET of the P-Cy3 sub-population, next we examined the D-Cy3 ($E_{D\bullet 601D} = 0.26$) sub-population of molecules (Figure 1H and Supplementary Figure S2B4). Close inspection of single molecule trajectories obtained in the presence of HsRAD51 and ATP revealed frequent high FRET excursions ($E_{RAD51} > 0.26$) in addition to low FRET transitions expected for a pure HsRAD51 catalyze DNA unwrapping mechanism (Supplementary Figure S13E–G). Overlaying the remodeling smFRET histogram with the histogram obtained from the control experiments revealed a clear right side (high FRET) broadening (Supplementary Figure S13H) further supporting our hypothesis that the DNA unwrapping is associated with the HO sliding/rotational motion (36) during HsRAD51catalyzed nucleosome remodeling (Supplementary Figure S13I).

DISCUSSION

HsRAD51 plays a central role in the initiation of HR, which leads to faithful repair of damage-induced DSBs as well as the generation of genetic diversity (4). Here we have focused on nucleosome dynamics during the formation of an HsRAD51-dsDNA NPF with high spatiotemporal resolution. As a molecular ruler smFRET provided a unique advantage to visualize these dynamics since the dimensions of the mononucleosomes (1) are comparable to the distance range where the FRET is most sensitive (10–100 Å) (26,30,31,34). Furthermore, while HsRAD51 may present mostly as heptametrical rings in the solution (4) it largely binds to dsDNA as a trimer, where each monomer occupies a defined footprint of 3 bp (9,11). Thus, HsRAD51 binding must occur in multiple steps to provoke remodeling dynamics that can be easily captured using real time smFRET.

Four nucleosome FRET constructs that were used in this study allowed us to map nucleosome-remodeling activity relative to three different locations on the nucleosomal DNA. The use of two different NPS allowed us to test the sequence context dependence. Simple single molecule population analysis showed that the amount of remodeling observed in a given observation time (~20 min) depended on the position of the Cy5 fluorophore on the DNA (compare Figures 2 and 4), indicating a DNA unwrapping mechanism as opposed to a HO pushing mechanism. For example, if an HO pushing mechanism were to operate, we would expect to observe roughly the same amount of remodeling for both 601 NPS Fwd Entry-Exit–Cy5 Nuc and 601 NPS Dyad–Cy5 Nuc constructs (18). Since the entry-exit region of the DNA has more freedom to undergo thermally induced fraying from HO surface (37), HsRAD51 will likely commence nucleation onto this region followed by progression into the dyad region while detaching the DNA from the HO (Figure 5).

Our single molecule data reveal that this apparently unidirectional overall unwrapping process consists of a series of consecutive, reversible, sub-steps indicative of HsRAD51 association/dissociation due to DNA binding site competition by the HO (Figure 5). Moreover, imaging experiments done under the absence of or limiting ATP hydrolysis conditions reveal that ATP hydrolysis is required from the initial entry-exit region unwrapping stage to drive the overall reaction unidirectionally. It is possible that the dead end HsRAD51-dsDNA NPF formed when HsRAD51 in the NPF hydrolyze ATP to ADP prevent the reverse reaction, namely the rewrapping of the DNA, because HsRAD51 stays bound without further ATP turnover (9,11). The non-discrete dynamics observed in our data suggest a model in which the overall process is primarily driven by the thermal fluctuations of nucleosomal DNA (37). Moreover, HsRAD51 ATP hydrolysis appears to be a secondary fast step that prevents reversibility. Consistent with this hypothesis, the similar residence times observed for intermediate states in the 601 NPS Fwd Entry-Exit–Cy5 Nuc construct at different HsRAD51 concentrations imply an underlying HsRAD51-independent rate-limiting step for unwrapping. We regard it likely that HsRAD51 is unable to nucleate filament growth until the DNA becomes accessible by thermal fluctuations in a manner that is similar to RNA polymerases binding to chromatin DNA (38,39). Furthermore, the highly reversible FRET transitions detected in individual trajectories suggest that once HsRAD51 gains access to the DNA there may be a 'tug-of-war' with the HO which strives to preserve the bound NPS DNA until HsRAD51 can bind tightly utilizing ATP binding/hydrolysis. These unwrapping-rewrapping transitions appear similar to the

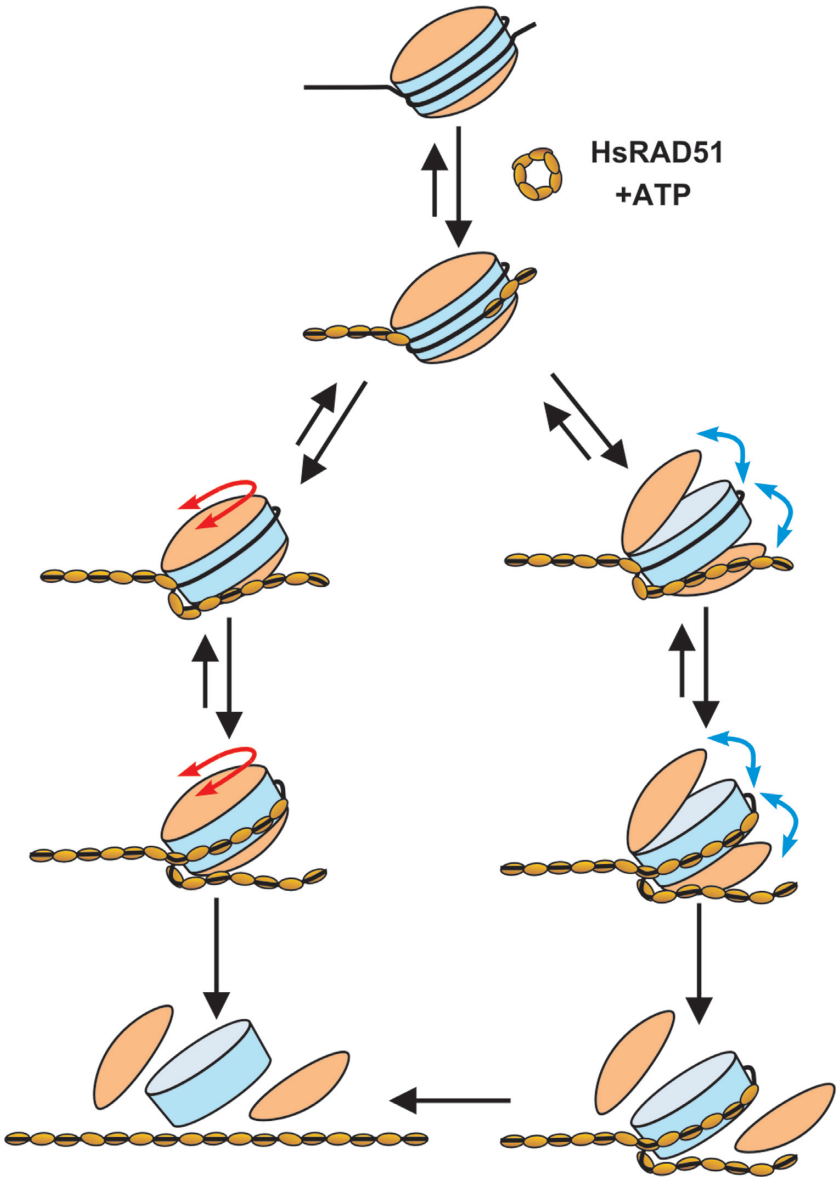

Figure 5. Model depicting the HO sliding/rotation-coupled nucleosomal DNA unwrapping by HsRAD51. HsRAD51 preferentially nucleates on the DNA from the entry-exit region, since it most likely to undergo thermally induced fraying from the HO surface. Because of the higher intrinsic interaction energy, the HO surface may rewrap the DNA by simple reoccupation following HsRAD51 dissociation, until HsRAD51 can form a stable NPF on the DNA. Once an NPF is nucleated onto entry-exit region, HsRAD51 may proceed with filament growth toward the dyad region while locally competing with HO to occupy the DNA. This competition to occupy the DNA will manifest as reversible dynamics in individual nucleosomes that appears as a 'tug-of-war' mechanism. However, thermal fluctuations of the DNA and ATP hydrolysis by HsRAD51 will ultimately favor the progression of NPF formation and the forward reaction. Our data also suggest that the removal of some DNA from the HO surface may lead to rapid sliding/rotational movements of the HO (red double head arrows) or reversible outward movement of $(H2A\text{-}H2B)_2$ (blue double head arrows). Eventually NPF formation will succeed in fully occupying the DNA, causing dissociation of the $(H2A\text{-}H2B)_2$ followed by the H3-H4 tetramer, or the complete and irreversible dissociation of the entire HO from the DNA in a single step.

force-induced transitions observed by Ngo *at al*. (34), suggesting that HsRAD51 may be capable of generating forces of up to ∼10 pN during oligomerization on dsDNA.

As suggested by our previous ensemble studies, the single molecule data presented here show that the progression of HsRAD51 NPF leads to the eviction of HO from the NPS. During this time we observed stable zero or near-zero FRET states composed of active Cy5 signals on the NPS and active Cy3 signals on H2A (HO). These results indicate the presence of partially unwrapped nucleosomes with inter-fluorophore distances >100 Å (26,30,31,34). The presence of active Cy3 signal indicates the presence of H2A on the DNA. Because it is well established that H2A-H2B histones are the least strongly bound histones in HO (18), it is reasonable to assume that the entire HO is still present on the DNA in these partially unwrapped reaction intermediates. We conclude that the FRET decays up to the generation of zero FRET states are due to DNA unwrapping and not due to histone dissociation. Our single molecule salt jump experiments further supported this notion by re-

vealing partially DNA unwrapped intermediate states prior to the dissociation of $(H2A\text{-}H2B)_2$ or the entire HO. It is most probable that $(H2A\text{-}H2B)_2$ would be removed from the DNA followed by the removal of $(H3\text{-}H4)_2$ during the gradual progression of HsRAD51 NPS compare to the removal of the entire HO (18). However we cannot rule-in or rule-out either of these models with the current experimental system, where there is no marker indicating the presence of H3 or H4 on the DNA.

Remodeling experiments performed with the 5S NPS Fwd Entry-Exit–Cy5 Nuc or the 601 NPS Rev Entry-Exit–Cy5 Nuc showed that regardless of the sequence or the presence of a linker DNA, HsRAD51 can readily catalyze nucleosome remodeling. Taken together with ATP hydrolysis data, this observation appears to suggest that the dysregulation of HsRAD51 localization can lead to irreversible remodeling of nucleosomes in the cells. These results also underline the importance of other enzymes such as HsRAD54, which may required to remove dead end HsRAD51-dsDNA NPFs (15,16).

Interestingly, the unique bidirectional $\sim 1\ s^{-1}$ FRET oscillations observed in the P-Cy3 and D-Cy3 subpopulations of the 601 Dyad–Cy5 Nuc construct appear similar to the histone octamer sliding movements observed with the nucleosome remodeler ACF (30). We consider at least two possibilities for these FRET oscillations: (i) HsRAD51 might simultaneously form an NPF on either side of the dyad region either beginning at the two entry-exit regions and/or on either side of the dyad region that could in principal create a torque, producing rapid rotational dynamics on the HO as proposed in a recent study that modeled the force induced unwrapping of nucleosomes (36), or (ii) the HsRAD51 NPF might induce a rapidly reversible outward motion of $(H2A\text{-}H2B)_2$ as pointed out by Lugar and coworkers (32) (Figure 5). We note that reversible $(H2A\text{-}H2B)_2$ outward movements should produce FRET oscillations between the initial and low FRET states but not above the initial FRET (32) (Figure 5). Regardless, these observations suggest that the initial formation of an HsRAD51 NPF on nucleosomal DNA results in unusual FRET oscillations indicative of distance changes between the NPS DNA and the HO around the dyad region (Supplementary Figure S1C, bottom panel and Supplementary Figure S13I). Apparent lack of these oscillations in entry-exit constructs might be due to the saturated initial FRET values and/or to masking by the large-scale FRET dynamics created by unwrapping-rewrapping of DNA exclusively.

Altogether our data reveal that although tightly assembled, nucleoprotein complexes such as nucleosomes can indeed consume thermal energy to undergo stochastic dynamic transitions. Enzymes such as HsRAD51 may utilize these dynamic transitions to enhance biochemical reactions. Our data further suggest that HsRAD51 NPF which may form on nucleosome bound dsDNA can have profound effects on the dynamic nature of nucleosomes, and may even facilitate the recruitment of other factors such as homologous HsRAD51-ssDNA NPFs or HsRAD54. Further high-resolution single molecule studies may be employed to test these hypotheses and dissect the underlying molecular events in details.

SUPPLEMENTARY DATA

Supplementary Data are available at NAR Online.

ACKNOWLEDGEMENTS

We would like to thank our laboratory members for insights and helpful discussions.

FUNDING

National Institutes of Health [GM080176 to R.F.]; Funding for open access charge: National Institutes of Health [GM080176].
Conflict of interest statement. None declared.

REFERENCES

1. McGinty,R.K. and Tan,S. (2015) Nucleosome structure and function. *Chem. Rev.*, **115**, 2255–2273.
2. McGinty,R.K. and Tan,S. (2016) Recognition of the nucleosome by chromatin factors and enzymes. *Curr. Opin. Struct. Biol.*, **37**, 54–61.
3. Seeber,A., Hauer,M. and Gasser,S.M. (2013) Nucleosome remodelers in double-strand break repair. *Curr. Opin. Genet. Dev.*, **23**, 174–184.
4. Amunugama,R. and Fishel,R. (2012) Homologous recombination in eukaryotes. *Prog. Mol. Biol. Transl. Sci.*, **110**, 155–206.
5. Jasin,M. and Rothstein,R. (2013) Repair of strand breaks by homologous recombination. *Cold Spring Harb. Perspect. Biol.*, **5**, a012740–a012758.
6. White,C.I. and Haber,J.E. (1990) Intermediates of recombination during mating type switching in Saccharomyces cerevisiae. *EMBO J.*, **9**, 663–673.
7. Sinha,M. and Peterson,C.L. (2008) A Rad51 presynaptic filament is sufficient to capture nucleosomal homology during recombinational repair of a DNA double-strand break. *Mol. Cell*, **30**, 803–810.
8. Alexiadis,V. and Kadonaga,J.T. (2002) Strand pairing by Rad54 and Rad51 is enhanced by chromatin. *Genes Dev.*, **16**, 2767–2771.
9. Hilario,J., Amitani,I., Baskin,R.J. and Kowalczykowski,S.C. (2009) Direct imaging of human Rad51 nucleoprotein dynamics on individual DNA molecules. *Proc. Natl. Acad. Sci. U.S.A.*, **106**, 361–368.
10. Amunugama,R., He,Y., Willcox,S., Forties,R.A., Shim,K.S., Bundschuh,R., Luo,Y., Griffith,J. and Fishel,R. (2012) RAD51 protein ATP cap regulates nucleoprotein filament stability. *J. Biol. Chem.*, **287**, 8724–8736.
11. Tombline,G., Heinen,C.D., Shim,K.S. and Fishel,R. (2002) Biochemical characterization of the human RAD51 protein. III. Modulation of DNA binding by adenosine nucleotides. *J. Biol. Chem.*, **277**, 14434–14442.
12. Jensen,R.B., Carreira,A. and Kowalczykowski,S.C. (2010) Purified human BRCA2 stimulates RAD51-mediated recombination. *Nature*, **467**, 678–683.
13. Thorslund,T., McIlwraith,M.J., Compton,S.A., Lekomtsev,S., Petronczki,M., Griffith,J.D. and West,S.C. (2010) The breast cancer tumor suppressor BRCA2 promotes the specific targeting of RAD51 to single-stranded DNA. *Nat. Struct. Mol. Biol.*, **17**, 1263–1265.
14. Tarsounas,M., Davies,D. and West,S.C. (2003) BRCA2-dependent and independent formation of RAD51 nuclear foci. *Oncogene*, **22**, 1115–1123.
15. Mazin,A.V., Mazina,O.M., Bugreev,D.V. and Rossi,M.J. (2010) Rad54, the motor of homologous recombination. *DNA Repair (Amst)*, **9**, 286–302.
16. Wright,W.D. and Heyer,W.D. (2014) Rad54 functions as a heteroduplex DNA pump modulated by its DNA substrates and Rad51 during D loop formation. *Mol. Cell*, **53**, 420–432.
17. Gildemeister,O.S., Sage,J.M. and Knight,K.L. (2009) Cellular redistribution of Rad51 in response to DNA damage: novel role for Rad51C. *J. Biol. Chem.*, **284**, 31945–31952.
18. North,J.A., Amunugama,R., Klajner,M., Bruns,A.N., Poirier,M.G. and Fishel,R. (2013) ATP-dependent nucleosome unwrapping catalyzed by human RAD51. *Nucleic Acids Res.*, **41**, 7302–7312.

19. Luger,K., Rechsteiner,T.J. and Richmond,T.J. (1999) Expression and purification of recombinant histones and nucleosome reconstitution. *Methods Mol. Biol.*, **119**, 1–16.
20. Yang,J.G., Madrid,T.S., Sevastopoulos,E. and Narlikar,G.J. (2006) The chromatin-remodeling enzyme ACF is an ATP-dependent DNA length sensor that regulates nucleosome spacing. *Nat. Struct. Mol. Biol.*, **13**, 1078–1083.
21. Dyer,P.N., Edayathumangalam,R.S., White,C.L., Bao,Y., Chakravarthy,S., Muthurajan,U.M. and Luger,K. (2004) Reconstitution of nucleosome core particles from recombinant histones and DNA. *Methods Enzymol.*, **375**, 23–44.
22. Tang,Y.C., Chang,H.C., Chakraborty,K., Hartl,F.U. and Hayer-Hartl,M. (2008) Essential role of the chaperonin folding compartment in vivo. *EMBO J.*, **27**, 1458–1468.
23. Baumann,P., Benson,F.E., Hajibagheri,N. and West,S.C. (1997) Purification of human Rad51 protein by selective spermidine precipitation. *Mutat. Res.*, **384**, 65–72.
24. Jeong,C., Cho,W.K., Song,K.M., Cook,C., Yoon,T.Y., Ban,C., Fishel,R. and Lee,J.B. (2011) MutS switches between two fundamentally distinct clamps during mismatch repair. *Nat. Struct. Mol. Biol.*, **18**, 379–385.
25. Senavirathne,G., Jaszczur,M., Auerbach,P.A., Upton,T.G., Chelico,L., Goodman,M.F. and Rueda,D. (2012) Single-stranded DNA scanning and deamination by APOBEC3G cytidine deaminase at single molecule resolution. *J. Biol. Chem.*, **287**, 15826–15835.
26. Senavirathne,G., Bertram,J.G., Jaszczur,M., Chaurasiya,K.R., Pham,P., Mak,C.H., Goodman,M.F. and Rueda,D. (2015) Activation-induced deoxycytidine deaminase (AID) co-transcriptional scanning at single-molecule resolution. *Nat. Commun.*, **6**, 10209–10220.
27. Senavirathne,G., Liu,J., Lopez,M.A. Jr, Hanne,J., Martin-Lopez,J., Lee,J.B., Yoder,K.E. and Fishel,R. (2015) Widespread nuclease contamination in commonly used oxygen-scavenging systems. *Nat. Methods*, **12**, 901–902.
28. Vafabakhsh,R., Levitz,J. and Isacoff,E.Y. (2015) Conformational dynamics of a class C G-protein-coupled receptor. *Nature*, **524**, 497–501.
29. McKinney,S.A., Joo,C. and Ha,T. (2006) Analysis of single-molecule FRET trajectories using hidden Markov modeling. *Biophys. J.*, **91**, 1941–1951.
30. Blosser,T.R., Yang,J.G., Stone,M.D., Narlikar,G.J. and Zhuang,X. (2009) Dynamics of nucleosome remodelling by individual ACF complexes. *Nature*, **462**, 1022–1027.
31. Deindl,S., Hwang,W.L., Hota,S.K., Blosser,T.R., Prasad,P., Bartholomew,B. and Zhuang,X. (2013) ISWI remodelers slide nucleosomes with coordinated multi-base-pair entry steps and single-base-pair exit steps. *Cell*, **152**, 442–452.
32. Bohm,V., Hieb,A.R., Andrews,A.J., Gansen,A., Rocker,A., Toth,K., Luger,K. and Langowski,J. (2011) Nucleosome accessibility governed by the dimer/tetramer interface. *Nucleic Acids Res.*, **39**, 3093–3102.
33. Lowary,P.T. and Widom,J. (1998) New DNA sequence rules for high affinity binding to histone octamer and sequence-directed nucleosome positioning. *J. Mol. Biol.*, **276**, 19–42.
34. Ngo,T.T., Zhang,Q., Zhou,R., Yodh,J.G. and Ha,T. (2015) Asymmetric unwrapping of nucleosomes under tension directed by DNA local flexibility. *Cell*, **160**, 1135–1144.
35. Hall,M.A., Shundrovsky,A., Bai,L., Fulbright,R.M., Lis,J.T. and Wang,M.D. (2009) High-resolution dynamic mapping of histone-DNA interactions in a nucleosome. *Nat. Struct. Mol. Biol.*, **16**, 124–129.
36. Dobrovolskaia,I.V. and Arya,G. (2012) Dynamics of forced nucleosome unraveling and role of nonuniform histone-DNA interactions. *Biophys. J.*, **103**, 989–998.
37. Widom,J. (2001) Role of DNA sequence in nucleosome stability and dynamics. *Q. Rev. Biophys.*, **34**, 269–324.
38. Hodges,C., Bintu,L., Lubkowska,L., Kashlev,M. and Bustamante,C. (2009) Nucleosomal fluctuations govern the transcription dynamics of RNA polymerase II. *Science*, **325**, 626–628.
39. Bintu,L., Kopaczynska,M., Hodges,C., Lubkowska,L., Kashlev,M. and Bustamante,C. (2011) The elongation rate of RNA polymerase determines the fate of transcribed nucleosomes. *Nat. Struct. Mol. Biol.*, **18**, 1394–1399.